Research Square

Preprints are preliminary reports that have not undergone peer review.
They should not be considered conclusive, used to inform clinical practice,
or referenced by the media as validated information.

Longer Telomeres Enhance the Ovarian Repair Capacity of Human Umbilical Cord Mesenchymal Stem Cells in Primary Ovarian Insufficiency

Huiling Bi
Changzhi Medical College Peace Hospital
Wuqing HU
Changzhi Medical College Peace Hospital
Zijing Wei
Changzhi Medical College Peace Hospital
Congxiu Miao
Changzhi Medical College Peace Hospital
Quanxi Li
quanxili@illinois.edu

Changzhi Medical College Peace Hospital

Research Article

Keywords: Primary ovarian insufficiency, Human umbilical cord-derived mesenchymal stem cells, Telomere length, Proteomics, Ovarian repair, IHNBA, CXCL6

Posted Date: November 17th, 2026

DOI: https://doi.org/10.21203/rs.3.rs-11145802/v1

License: This work is licensed under a Creative Commons Attribution 4.0 International License.
Read Full License

Additional Declarations: No competing interests reported.

Longer Telomeres Enhance the Ovarian Repair Capacity of Human Umbilical Cord Mesenchymal Stem Cells in Primary Ovarian Insufficiency

Huiling Bi[1,#], Wuqing Hu[1,#], Zijing Wei[1], Congxiu Miao[1,*] and Quanxi Li[1,2,*],

[1]Department of Reproductive Genetics, Heping Hospital of Changzhi Medical School, Key Laboratory of Reproduction Engineer of Shanxi Health Committee, Changzhi, Shanxi 046000, China. [2]Department of Comparative Bioscience, Collage of Veterinary Medicine, University of Illinois at Urbana-Champaign. 2001 S Lincoln Ave. Urbana, IL 61802.

Bi Huiling, chenbihuiling@163.com; Hu Wuqing, 531544380@qq.com; Wei Zijing 734502013@qq.com ; Miao Congxiu cxms@163.com, and Li Quanxi qanxili@czmc.edu.cn

# equal contribution; * Corresponding authors

Short title: Longer Telomeres Enhance hUC-MSCs Ovarian Repair

Summary sentence: Long-telomere hUC-MSCs exhibit enhanced secretory activity, stronger regenerative potential, and superior ovarian repair in POI models, supporting telomere length as a practical potency biomarker for MSC quality, consistency, and therapeutic efficacy.

Keywords: Primary ovarian insufficiency; Human umbilical cord-derived mesenchymal stem cells; Telomere length; Proteomics; Ovarian repair, IHNBA, CXCL6

Name and address of person to whom reprint requests should be addressed: Quanxi Li, E-mail: quanxili@illinois.edu Comparative Bioscience, Collage of Comparative Biosciences, University of Illinois at Urbana-Champaign. 2001 S Lincoln Ave. Urbana, IL 61802.

Abstract

Background: Human umbilical cord-derived mesenchymal stem cells (hUC-MSCs) have shown promise for treating primary ovarian insufficiency (POI), but biomarkers that predict their therapeutic potency remain unclear. This study investigated the relationship between telomere length and the biological characteristics and therapeutic efficacy of hUC-MSCs in POI. **Methods:** Telomere length was measured in 50 independent hUC-MSC preparations. Cells with the longest and shortest telomeres were selected for comparison of proliferation, migration, differentiation, secretory function, and therapeutic efficacy in a cyclophosphamide-induced rat model of POI. Proteomic analysis was performed to identify telomere length-associated secreted proteins. **Results:** Long-telomere hUC-MSCs exhibited significantly greater proliferative and migratory capacities than short-telomere cells while maintaining comparable differentiation potential. Proteomic analysis identified 204 differentially expressed proteins, including increased expression of C-X-C motif chemokine ligand 6 (CXCL6) and Inhibin beta A (INHBA) in long-telomere hUC-MSCs. In vivo, hUC-MSC transplantation improved ovarian morphology and endocrine function in POI rats. Compared with short-telomere hUC-MSCs, long-telomere cells produced greater reductions in serum follicle-stimulating hormone levels, higher anti-Müllerian hormone concentrations, improved follicular preservation, and increased ovarian expression of CXCL6 and INHBA. **Conclusions:** Telomere length is closely associated with the biological activity, secretory profile, and therapeutic efficacy of hUC-MSCs. Long-telomere hUC-MSCs demonstrate superior ovarian repair capacity, suggesting that telomere length may serve as a potential biomarker for hUC-MSC quality assessment and potency prediction, thereby facilitating the optimization of stem cell-based therapies for POI.

Introduction

Human umbilical cord-derived mesenchymal stem cells (hUC-MSCs) are multipotent stromal cells isolated from Wharton's jelly of the umbilical cord. Like other mesenchymal stem cell populations, hUC-MSCs exhibit low immunogenicity owing to their lack of major histocompatibility complex class II (MHC-II/HLA class II) expression [1–4]. Because of their ease of acquisition, high proliferative capacity, multilineage differentiation potential, low immunogenicity, and minimal ethical concerns, hUC-MSCs have attracted considerable attention in the field of regenerative medicine [1–4].

Accumulating evidence suggests that the therapeutic effects of hUC-MSCs are mediated primarily through paracrine mechanisms rather than direct replacement of damaged tissues [5]. hUC-MSCs release bioactive soluble factors, including growth factors, cytokines, extracellular vehicles and exosomes [5–8]. Through complex cell-to-cell communication, these factors modulate immune responses, suppress excessive inflammation, promote cellular survival, and regulate the functions of neighbouring cells. In addition, hUC-MSCs exert anti-apoptotic, anti-fibrotic, and antioxidative effects, thereby preventing tissue degeneration and facilitating functional recovery [5–8].

Premature ovarian failure, currently referred to as primary ovarian insufficiency (POI), is a severe gynecologically endocrine disorder characterized by ovarian follicular depletion or dysfunction before the age of 40 years [9,10]. Clinically, POI is associated with menstrual irregularities or amenorrhea, elevated follicle-stimulating hormone (FSH) levels, reduced estradiol (E2), progesterone (P4) and anti-Müllerian hormone (AMH) levels, infertility, and various menopausal symptoms [9,10]. Although hormone replacement therapy remains the primary clinical intervention, current treatments are unable to fully restore ovarian reserve or recover normal ovarian function.

In recent years, mesenchymal stem cell-based therapies have emerged as promising strategies for the treatment of POI. hUC-MSCs have demonstrated remarkable therapeutic potential in both preclinical and clinical studies [11–13]. Rather than directly generating new oocytes, transplanted hUC-MSCs improve the ovarian microenvironment through multiple mechanisms. These include protecting granulosa cells, suppressing apoptosis and ferroptosis, regulating oxidative stress, and enhancing follicular survival through the secretion of trophic and antioxidative factors. Furthermore, hUC-MSC transplantation has been shown to promote follicular development, restore ovarian morphology, increase serum AMH and E2 levels, and reduce elevated FSH concentrations [14,15]. The paracrine secretome released by hUC-MSCs also contributes to anti-inflammatory and anti-fibrotic responses, thereby improving the ovarian niche and facilitating tissue regeneration. Despite these encouraging findings, reliable molecular biomarkers for assessing the quality and therapeutic potency of hUC-MSC products remain largely unavailable. Identification of such biomarkers is critical for standardizing stem cell manufacturing and predicting clinical efficacy.

Telomere length has emerged as a potentially important indicator of mesenchymal stem cell (MSC) quality [16,17]. Telomeres are repetitive nucleotide sequences located at the ends of chromosomes that protect genomic integrity and support the long-term proliferative and regenerative capacity of stem cells. During repeated cell divisions, particularly under extended in vitro culture conditions, telomeres progressively shorten. Once a critical telomere length is reached, cells undergo replicative senescence, resulting in impaired proliferation, reduced differentiation potential, and compromised regenerative function [16,17]. Although telomere length is widely regarded as a marker of cellular aging and replicative capacity, its predictive value for hUC-MSC proliferation, differentiation potential, immunomodulatory activity, and clinical efficacy has not been fully established. Further investigation is therefore required to

93 determine whether telomere length can serve as a reliable biomarker for assessing hUC-MSC
94 quality and therapeutic potency.

95 To address this knowledge gap, the proliferation and differentiation potential of hUC-MSCs
96 with different telomere lengths were assessed. Data-independent acquisition (DIA)-based
97 proteomic analysis was employed to characterize telomere length-associated alterations in the
98 secretory and functional profiles of hUC-MSCs. Furthermore, the therapeutic efficacy of hUC-
99 MSCs with different telomere lengths was evaluated in a rat model of POI. Our findings
100 demonstrated that hUC-MSCs with longer telomeres exhibited a superior capacity to restore
101 ovarian function, as evidenced by improved follicular development, enhanced ovarian reserve,
102 and recovery of endocrine function. These results suggest that telomere length is closely
103 associated with the regenerative potential of hUC-MSCs and may serve as a valuable biomarker
104 for predicting the quality, potency, and therapeutic efficacy of MSC-based products.

105

106 **Materials and Methods**

107 **Isolation and Culture of hUC-MSCs**

108 The human umbilical cord tissue used for isolation of hUC-MSCs was obtained from healthy
109 full-term deliveries after written informed consent from mothers, and the study was conducted
110 in accordance with the principles of the Declaration of Helsinki and was approved by the Ethics
111 Committee of Changzhi Medical school (Approval No. 2021-043). Umbilical cords were
112 obtained from Eligible donors were 25-30 years of age, had no history of malignancy or major
113 surgery, and were free of pregnancy-related complications, including gestational hypertension,
114 preeclampsia, gestational diabetes mellitus, and hypothyroidism. Maternal serological
115 screening results for human immunodeficiency virus, hepatitis B virus, and syphilis were

negative within one month before delivery. Newborns with birth weights >2,500 g and without congenital abnormalities were included.

Approximately 10 cm of umbilical cord tissue was collected under sterile conditions. After removal of blood vessels and the outer membrane, Wharton's jelly was dissected, minced into 3-5 mm^3 fragments, and evenly distributed in T75 culture flasks. The explants were cultured in serum-free medium at 37°C in a humidified atmosphere containing 5% CO_2. The culture medium was completely replaced on day 7 and subsequently every 3 days. Cell morphology and growth were monitored using an inverted microscope. Cells were passaged upon reaching 70-80% confluence and designated as passage 1 (P1).

Flow Cytometric Analysis of Cell Surface Markers

Passage 5 (P5) hUC-MSCs were subjected to flow cytometry. Briefly, cells were harvested and resuspended in staining buffer. Aliquots of 100 μL cell suspension were incubated with FITC-conjugated antibodies against CD73, CD90, CD105, CD31, CD34, CD45, CD19, CD11b, and HLA-DR (see Supplementary Table S1), respectively. Following incubation and washing, cell surface marker expression was analysed by flowcytometry according to the manufacturer's instructions.

Cell Proliferation Assay

Cell proliferation was assessed using an Enhanced Cell Counting Kit-8 (CCK-8; E-CK-A362, Elabscience Biotechnology Co., Ltd., Wuhan, China) [18]. Briefly, 100 μL of cell suspension was seeded into each well of a 96-well plate with five replicate wells per group. Wells containing culture medium without cells served as blank controls. At the indicated time points, CCK-8 reagent was added according to the manufacturer's protocol. Absorbance was measured

using a microplate reader, and growth curves were generated using GraphPad Prism 10.0 software.

Adipogenic and Osteogenic Differentiation

For adipogenic differentiation, hUC-MSCs were seeded into 0.1% gelatin-coated six-well plates at a density of 2×10^4 cells/cm². Upon reaching full confluence, cells were cultured in adipogenic induction medium (OriCell Therapeutics, Shanghai, China). After 21 days of induction, cells were fixed and stained with Oil Red O to visualize intracellular lipid droplets.

For osteogenic differentiation, hUC-MSCs at approximately 60% confluence were cultured in osteogenic induction medium (OriCell Therapeutics, Shanghai, China) for 14 days. Cells were then fixed and stained with Alizarin Red S solution. Mineralized calcium nodules were examined microscopically to evaluate osteogenic differentiation.

Wound Healing Assay

hUC-MSCs were seeded into 12-well plates at a density of 2×10^5 cells/well. After reaching complete confluence, a linear wound was generated using a sterile pipette tip. Detached cells were removed by washing with PBS, and serum-free medium was added. Images of the wound gaps were captured at 0, 12, and 24 h using an inverted microscope. Cell migration was quantified according to the following formula: Wound closure (%) = $[(W_0 - Wt)/W_0] \times 100$ where W_0 represents the initial wound width and Wt represents the wound width at the indicated time point [18].

Telomere Length Measurement

Mean telomere length was determined using Terminal Restriction Fragment analysis [19]. Briefly, genomic DNA was digested with restriction enzymes and separated by agarose gel

electrophoresis. DNA fragments were transferred onto nylon membranes and hybridized with a digoxigenin-labelled telomere-specific probe. Hybridization signals were detected using anti-DIG alkaline phosphatase conjugate according to the manufacturer's protocol. The resulting images were analysed using TeloTool software (MATLAB Central) to calculate average telomere length [20].

Data-Independent Acquisition (DIA) mass spectrometry proteomic analysis

DIA-based proteomic analysis was performed by Majorbio Bio-Pharm Technology Co., Ltd. (Shanghai, China) [21]. Proteins were extracted from lyophilized conditioned media and digested with trypsin. Peptides were analysed using a Vanquish Neo liquid chromatography system coupled to an Orbitrap Astral mass spectrometer operating in data-independent acquisition (DIA) mode. The MS1 and MS2 scan ranges were set to 70-1050 m/z and 150-2000 m/z, respectively. Raw data were processed using Spectronaut™ 18 software. Search parameters included peptide lengths of 7-52 amino acids, Trypsin/P digestion specificity, protein false discovery rate (FDR) ≤1%, peptide FDR ≤1%, peptide confidence ≥99%, and XIC width ≤75 ppm. The mass spectrometry proteomics data have been deposited to the ProteomeXchange Consortium via the PRIDE partner repository, and the dataset is available with identifier PXD082583.

Data quality and reproducibility were evaluated by Pearson correlation analysis and Principal component analysis. Hierarchical clustering was performed based on normalized protein abundance values. Differentially expressed proteins (DEPs) were identified using the following criteria: Fold change ≥1.5 or ≤0.67; $P < 0.05$; Gene Ontology enrichment analysis was performed for biological process, cellular component, and molecular function categories. Kyoto Encyclopedia of Genes and Genomes (KEGG) pathway analysis was conducted to identify significantly enriched pathways.

Cyclophosphamide-Induced Rat Model of Primary Ovarian Insufficiency

Pathogen-free female Wistar rats (8 weeks old, 190-220 g) were obtained from Jinan Pengyue Laboratory Animal Breeding Co., Ltd. (License No. SCXK [Lu] 2022-0006). Animals were housed under standard laboratory conditions with free access to food and water. All procedures were approved by the Institutional Animal Care and Use Committee of Changzhi Medical College (Approval No. DW2021098).

Estrous cyclicity was monitored daily by vaginal smears for 7 consecutive days before enrolment. Female rats with the normal estrous cyclicity were chosen for the subsequent experiments. A primary ovarian insufficiency (POI) model was induced by intraperitoneal administration of cyclophosphamide (CTX) as described previously [22]. Rats received a loading dose of 50 mg/kg CTX on day 1 followed by 8 mg/kg/day CTX from days 2-14. Forty rats were randomly assigned to four groups (n = 10 per group) and treated as described in Figure 1A. Group A (LT group): POI + long-telomere hUC-MSCs; Group B (ST group): POI + short-telomere hUC-MSCs; Group C (POI group): POI + saline; Group D (CON group): Age-matched untreated control. Body weight, food intake, activity, fur appearance, and oestrous cyclicity were monitored throughout the experiment.

Ovarian Transplantation of hUC-MSCs

Following successful establishment of the POI model, rats were anesthetized with 2.5% tribromoethanol (10 mL/kg, intraperitoneally). Adequate anesthesia was confirmed by the absence of a response to appropriate external stimuli before the experimental procedures were performed. Bilateral ovaries were exposed through a dorsal incision [22]. Groups A and B received bilateral ovarian injections of long- or short-telomere hUC-MSCs, respectively. A total of 1×10^6 cells suspended in 40 μL sterile saline was administered per rat using a

microsyringe. Group C received bilateral ovarian injections of an equal volume of saline. The incision was closed with absorbable sutures, and animals were allowed to recover normally.

At the end of the experimental period, animals were euthanized by CO2 inhalation in a chamber with controlled delivery of CO2 in accordance with institutional animal-care guidelines and applicable ethical regulations. The procedure was selected to minimize pain and distress to the animals. Death was confirmed by trained personnel prior to tissue collection. Blood samples were collected for determination of FSH, AMH, E2, and P4 levels using commercial ELISA kits according to the manufacturers' instructions. Both ovaries were collected. One ovary was stored at −80°C, while the contralateral ovary was fixed in paraformaldehyde, embedded in paraffin, sectioned at 5 μm. The serial sections were mounted on a glass slide and stained with hematoxylin and eosin for histological evaluation. The numbers of oocyte containing follicles were counted in every 10th serial section under a light microscope as described previously [23]. Stage of follicular development was assessed using previously defined criteria. Briefly, primordial follicles contained the oocyte surrounded by a single layer of squamous granulosa cells, primary follicles contained the oocyte surrounded by a single layer of cuboidal granulosa cells, secondary follicles contained the oocyte surrounded by multiple layers of cuboidal granulosa cells with a fluid-filled antral space and theca cell layers. All primordial and primary follicles with oocytes, regardless of nuclear material in the oocytes, were counted.

Superovulation and Oocyte counting

Female rats first received 150 IU/kg body weight of pregnant mare serum gonadotropin (PMSG) via intraperitoneal injection to stimulate follicular development. Forty-eight hours later, 75 IU/kg body weight of human chorionic gonadotropin (hCG) was administered intraperitoneally to induce ovulation. At 13 to 15 hours after hCG administration, cumulus-oocyte complexes (COCs) were collected from the ampullae of the oviducts, cumulus cells were removed by

231 treatment with hyaluronidase, and the ovulated oocytes were examined and counted under a
232 dissecting microscope.

233 **Immunofluorescence Analysis**

234 Paraffin-embedded ovarian sections were deparaffinized, rehydrated, and subjected to antigen
235 retrieval in citrate buffer (pH 6.0). Sections were blocked with 3% hydrogen peroxide and
236 bovine serum albumin before incubation overnight at 4°C with primary antibodies against C-
237 X-C motif chemokine ligand 6 (CXCL6) or inhibin βA (INHBA) (see supplementary table S1).
238 After washing, sections were incubated with FITC-conjugated goat anti-rabbit secondary
239 antibody for 50 min at room temperature. Nuclei were counterstained with DAPI. 3-4 images
240 were acquired for each section under a fluorescence microscope, and the total fluorescent
241 intensities were analysed by Image J software [18].

242 **Statistical Analysis**

243 Data are presented as mean ± standard deviation (SD). Statistical analyses were performed
244 using GraphPad Prism 10.0 and SPSS 27.0. Data were tested for normality and homogeneity
245 of variance prior to analysis. Comparisons among multiple groups were performed using one-
246 way analysis of variance (ANOVA) followed by Tukey's post hoc test. A value of $P < 0.05$ was
247 considered statistically significant. Statistical significance was denoted as follows: ns, $P > 0.05$;
248 *$P < 0.05$; **$P < 0.01$; ***$P < 0.001$; and ****$P < 0.0001$.

249

Results

Effect of telomere length on proliferation and migration of hUC-MSCs

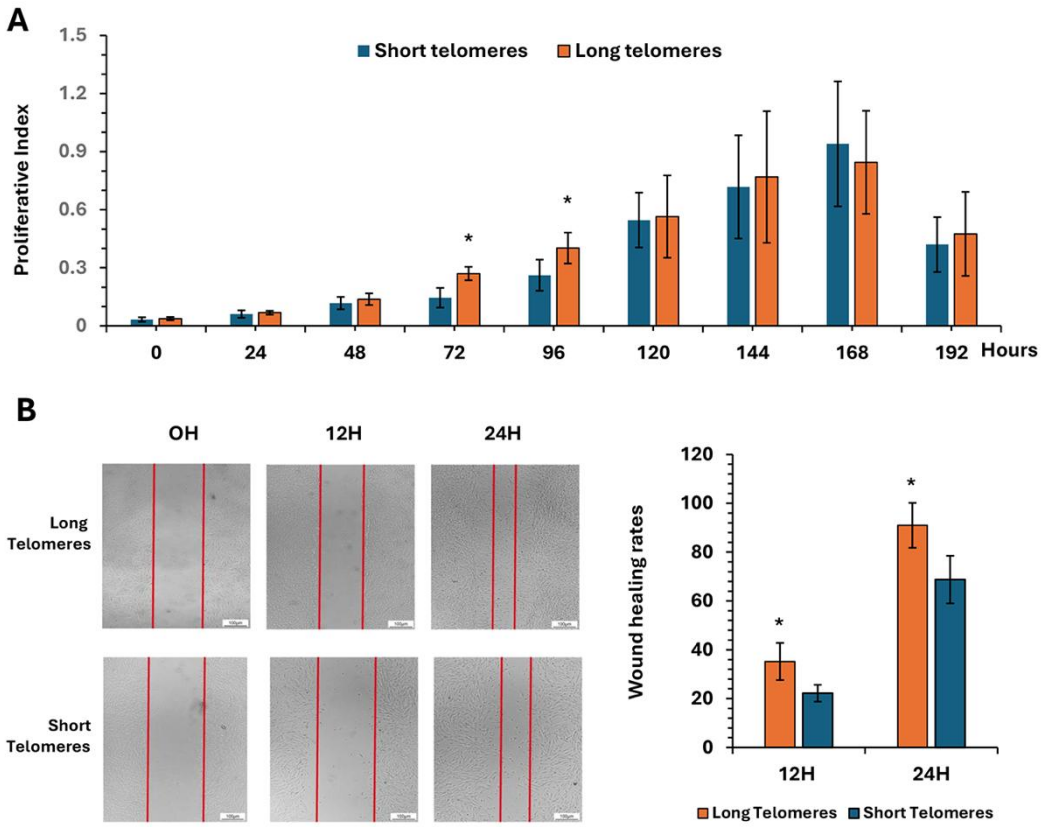
hUC-MSCs are characterized by their capacity for self-renewal, multilineage differentiation, and expression of specific mesenchymal surface markers. To verify the identity and purity of the isolated cells, flow cytometric analysis was performed to characterize the immunophenotype of hUC-MSCs at passage 5 (P5). As shown in Supplementary Figure 1, most hUC-MSCs are positive for mesenchymal markers, such as CD105 (100.0%), CD73 (99.9%), and CD90 (100.0%). In contrast, the number of cells that are positive for endothelial cell marker CD31 (0.49%), hematopoietic cell markers such as CD34 (0.32%), CD45 (0.56%), CD19 (0.10%), and CD11b (1.33%), as well as human leukocyte differentiation antigen class II (HLA-DR, 0.70%) are negligible. These findings demonstrate that the cells meet the immunophenotypic criteria for mesenchymal stem cells and exhibit high purity.

The biological characteristics of the isolated hUC-MSCs were further evaluated. Cell proliferative activity was assessed using the CCK-8 assay. As shown in Supplementary Figure 2A, hUC-MSC proliferation increased progressively from 24 to 168 h after seeding, reached a peak at 168 h, and subsequently declined at 196 h as the cells approached confluence. The multilineage differentiation potential of these cells was also examined (see Supplementary Figure 2B). Following adipogenic induction, abundant intracellular lipid droplets were detected by Oil Red O staining (Upper panel). Similarly, osteogenic induction resulted in extensive calcium deposition as demonstrated by Alizarin Red S staining (Lower panel). No obvious lipid droplets or calcium nodules were observed prior to differentiation induction. Collectively, these results confirmed the proliferative and multilineage differentiation capacities of the isolated hUC-MSCs.

To investigate the relationship between telomere length and cellular functions, genomic DNA was isolated from 50 independent hUC-MSC preparations, and telomere length was measured by terminal restriction fragment analysis, followed by Southern blot hybridization (see Supplementary Figure 3A). Quantitative analysis using TeloTool software revealed that the average telomere length ranged from 10.04 to 15.63 kb (see Supplementary Figure 3B). Uncropped, full-length blot images corresponding to the blots presented are provided in Supplementary Figure S6**.** Molecular-weight markers and relevant loading controls are included where applicable. Based on telomere length distribution, the top 10% of samples (red, n = 5) were selected as the long-telomere group, whereas the bottom 10% (blue, n = 5) were selected as the short-telomere group for subsequent analyses.

The proliferative and migratory capacities of hUC-MSCs with longest or shortest telomeres (n=5 per group) were subsequently compared. As shown in Figure 1A, both groups exhibited similar growth kinetics. However, cells with longer telomeres displayed moderately greater proliferative activity at 72 and 96 h compared with cells possessing shorter telomeres. Consistent with these findings, wound-healing analysis demonstrated an enhanced migratory activity in the long-telomere group, as evidenced by higher wound-closure rates (Figure 1B).

To determine whether telomere length influences differentiation potential, adipogenic and osteogenic differentiation assays were performed in hUC-MSCs with long or short telomeres. No significant differences in Oil Red O staining or Alizarin Red S staining were observed between the two groups (data not shown), indicating comparable adipogenic and osteogenic differentiation capacities in these cells. Taken together, these findings suggest that longer telomeres are associated with enhanced proliferative and migratory capacities of hUC-MSCs, while exerting minimal influence on their adipogenic and osteogenic differentiation potential.



298 **Figure 1.** Comparison of cellular proliferation and migration between hUC-MSCs with the
299 longest and shortest telomeres. **(A)** Cell proliferation was evaluated using the Cell Counting
300 Kit-8 (CCK-8) assay at the indicated time points. Proliferation indices are presented in the
301 graph. **B)** Cell migratory capacity of hUC-MSCs with the longest and shortest telomeres was
302 assessed using a wound-healing assay. Representative images of cell migration into the wound
303 area are shown in the left panel, and quantitative analysis of wound closure rates is presented
304 in the right panel. Data are expressed as mean ± SD (n = 5). $P < 0.05$.

305

Telomere length is associated with distinct secretory protein profiles in hUC-MSCs

To investigate whether telomere length influences the secretory characteristics of hUC-MSCs, the conditioned media from long-telomere and short-telomere hUC-MSCs (n = 5 per group) were subjected to DIA-based proteomic analysis. Serum-free conditioned media were collected from these cells, lyophilized, and analysed by mass spectrometry.

DIA-based proteomic analysis identified a total of 3,339 secreted proteins in the conditioned media of hUC-MSCs. To examine sample relationships, Pearson correlation analysis was performed. As shown in Figure 2A, strong correlations were observed among biological replicates within each group. Pearson correlation coefficients ranged from 0.875 to 0.952 in the long-telomere group and from 0.914 to 0.953 in the short-telomere group. In contrast, correlation coefficients between the two groups ranged from 0.734 to 0.784, indicating high reproducibility and consistency of the proteomic dataset and DIA proteomic analysis.

A Venn diagram was used to compare protein composition between long and short telomere groups (Figure 2C). Among the 3,339 proteins identified, 3,328 proteins (99.70%) were detected in both groups, indicating a high degree of overlap in secretome composition. Only two proteins (0.06%) were uniquely detected in the long-telomere group, including DEAD-box helicase 17 (DDX17) and cytosolic 5'-nucleotidase IIIA (NT5C3), whereas eight proteins (0.24%) were unique to the short-telomere group, including myosin light chain 11 (MYL11), Cytochrome c oxidase IV isoform 1 (COX4), MYH7, Semenogelin-2 (EMG2), and fumarate hydratase (FH). Hierarchical clustering analysis demonstrated that biological replicates clustered tightly within each group, whereas long- and short-telomere samples formed distinct clusters. One cluster exhibited increased expression in long-telomere hUC-MSCs and decreased expression in short-telomere cells, whereas the second cluster showed the opposite pattern (Figure 2B). These findings suggest that although the overall secretome composition

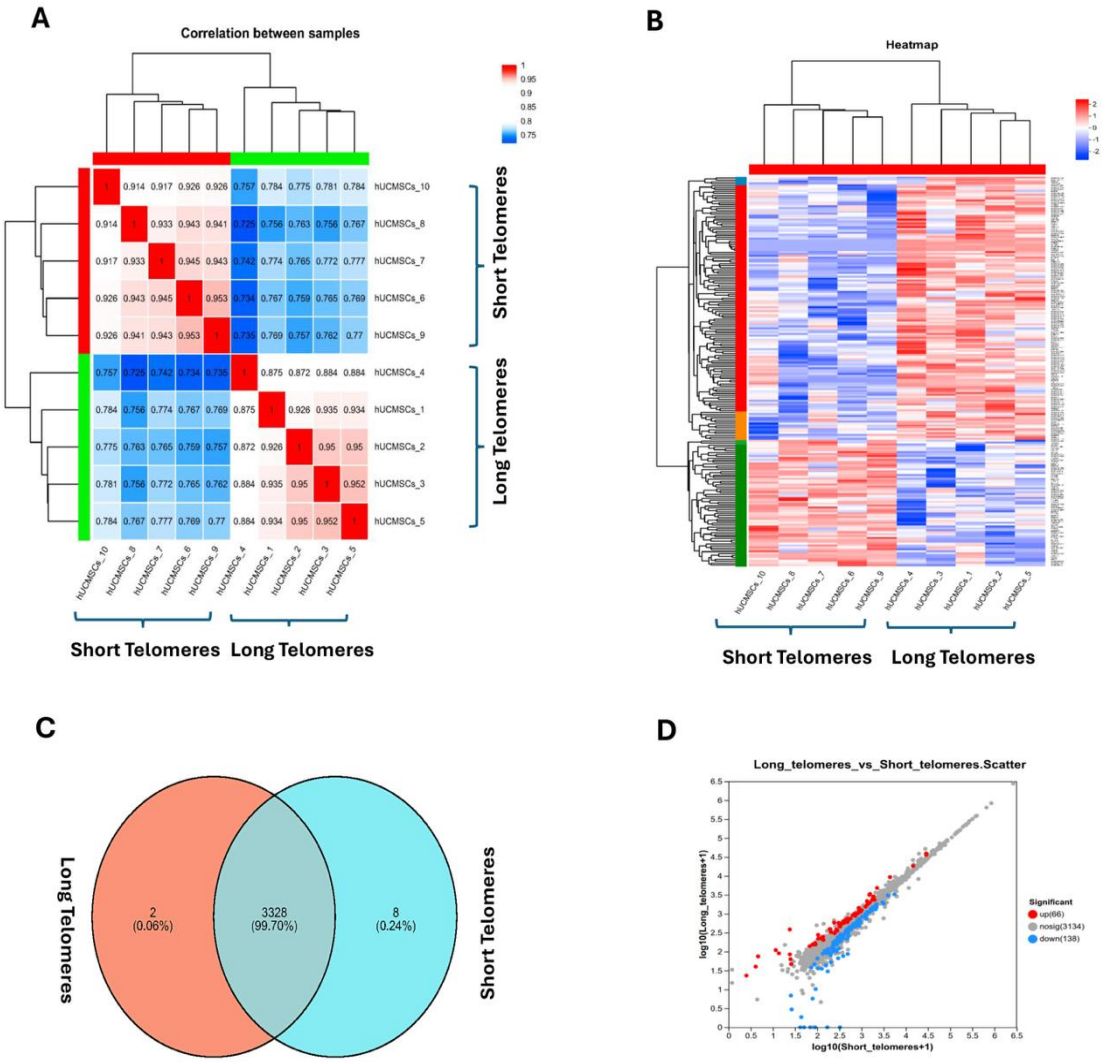


Figure 2. DIA-based proteomic analysis**. A.** Heatmap showing pairwise Pearson correlation coefficients among samples collected from long- and short-telomere hUC-MSCs. Samples clustered according to telomere status; Warmer colours indicate stronger correlations. **B.** Hierarchical clustering heatmap of differentially expressed proteins**.** Rows represent proteins and columns represent individual samples. Red indicates relatively high protein abundance, and blue indicates relatively low abundance. **C.** Venn diagram of proteins identified in the secretomes of long- and short-telomere hUC-MSCs. Of the 3,338 proteins identified, 3,328 proteins were shared between groups. **D.** Volcano plot of Differentially expressed proteins. Red dots indicate upregulated proteins, Blue dots indicate down regulated proteins, Gray dots indicate no significant changed proteins.

was highly conserved, telomere length influenced the expression of a small subset of proteins that may contribute to functional differences between cell populations.

Using thresholds of fold change ≥ 1.5 and $P < 0.05$, a total of 204 differentially expressed proteins (DEPs) were identified (Figure 2D). Among these, 66 proteins were upregulated (Table 1), and 138 proteins were downregulated (Table 2) in the long-telomere group compared with the short-telomere group. Representative proteins, such as C-X-C Motif Chemokine Ligand 6 (CXCL6)**,** Pentraxin 3 (PTX3**),** Fc Gamma Receptor IIA (FCGR2A**),** Interferon-Induced Transmembrane Protein 1 **(**IFITM1**)**, Lysyl Oxidase Like 1 (LOXL1)**,** Bone Morphogenetic Protein 1 (BMP1**),** Decorin (DCN), and Alpha Actinin 1 (ACTN1)**,** Inhibin beta A (INHBA), EF-Hand Domain Family Member D2 (EFHD2), and Centromere Protein C (CENPC). Kyoto Encyclopedia of Genes and Genomes (KEGG) pathway enrichment analysis revealed that the differentially secreted proteins were primarily related to cell growth and death, signal transduction, immune system regulation, transport and catabolism, and protein processing (see Supplementary Figure 4).

360 **Table 1.** List of that are upregulated proteins with known functions in the long telomere hUC-

361 MSCs.

Gene symbol	Protein Name	Fold Change	P- value
CENPC	Centromere Protein C	20.1811	0.000298
CXCL6	C-X-C motif chemokine, Granulocyte Chemotactic Protein 2 (GCP-2)	16.6529	0.02472
SPRR1A	Cornifin-A	12.6087	0.004545
LOXL1	Lysyl Oxidase-Like 1	10.2179	0.000973
EFHD2	EF-hand domain-containing protein D2	7.0187	0.01084
Cathepsin B	Cathepsin B	2.643	0.000303
BMP1	Metalloendopeptidase	2.5871	0.01037
KRT6C	Keratin, type II cytoskeletal 6C	2.4195	0.04476
DCN	Decorin	2.1525	0.04591
KRT6B	Keratin, type II cytoskeletal 6B	2.1086	0.02242
GLRX3	Glutaredoxin-3	2.092	0.02417
PAM	Peptidylglycine α-amidating monooxygenase	2.0736	0.005292
PTX3	Pentraxin-related protein PTX3	2.0654	0.001343
ATP6AP1	ATP6AP1	2.0518	0.0392
BBS7	BBS7	1.842	0.003613
IFITM1	Interferon-Induced Transmembrane Protein 1	1.8375	0.04183
PGM2L1	Glucose 1,6-bisphosphate synthase	1.6948	0.004618
INHBA	Inhibin beta A chain, a member of TGF beta family	1.6512	0.04011
ACTN1	Alpha-actinin-1	1.597	0.009295

362

363

364

365

366

367

368 **Table 2**. Down regulated proteins with known functions in long telomere hUC-MSC

Gene Symbol	Protein Name	Fold change	*P*-value
OIT3	Oncoprotein-induced transcript 3 protein	0.6483	0.04995
USP14	Ubiquitin carboxyl-terminal hydrolase	0.6354	0.04307
NUTF2	NUTF2	0.5966	0.0385
PYGL	Glycogen phosphorylase, liver form	0.5928	0.01245
hCG_2014768	Translation machinery-associated protein 7	0.5883	0.004381
SSR4	Translocon-associated protein subunit delta	0.5829	0.01954
DPP3	Dipeptidyl peptidase 3	0.5782	0.02734
SLC3A2	SLC3A2	0.5753	0.02808
FUBP1	Far Upstream Element-Binding Protein 1	0.5539	0.03556
PPP2R2C	B55γ regulatory subunit of Protein Phosphatase 2A (PP2A)	0.5306	0.006865
RPS3A	40S ribosomal protein S3a	0.5247	0.04222
CAMK1	CAMK1	0.4881	0.03722
HNRNPH1	HNRNPH1	0.4566	0.04484
CASP8AP2	CASP8AP2	0.4436	0.03157
RUVBL1/RUVBL2	RuvB-like helicase	0.4283	0.004103
HNRNPM	Heterogeneous nuclear ribonucleoprotein M	0.4004	0.03211
HNRNPH2	Heterogeneous nuclear ribonucleoprotein H2	0.2559	0.003518
SLC25A3	Phosphate carrier protein, mitochondrial	0.2219	0.04891
RPS25	40S ribosomal protein S25	0.1746	0.04857
PRH1	PRH1	0.1683	0.01523
NES	NES	0.1013	0.02861
UQCRC2	UQCRC2	0.06055	0.005306
MYL11	MYL11	1.00E-05	0.008752
FH	Fumarate hydratase, mitochondrial	1.00E-05	0.000247
MYH7	MYH7	1.00E-05	0.007966
SEMG2	Semenogelin-2	1.00E-05	0.02225
COX4I1	Cytochrome c oxidase subunit 4	1.00E-05	0.03557

369 Reactome pathway analysis showed that the DEPs between hUC-MSCs with the longest and
370 shortest telomeres were predominantly enriched in pathways related to metabolism of proteins,
371 developmental biology, extracellular matrix organization, and signal transduction. Additional
372 enrichment was observed in immune system and innate immune system pathways, post-
373 translational protein modification, regulation of IGF transport and uptake, platelet
374 degranulation, and haemostasis (see Supplementary Figure 5). These results indicate that
375 telomere length is associated with broad alterations in the hUC-MSC secretome, that may be
376 involved in tissue remodelling, cellular signalling, immune regulation, and regenerative
377 processes.

hUC-MSCs with longer telomeres exhibit enhanced therapeutic efficacy in a rat model of primary ovarian insufficiency

To evaluate the therapeutic efficacy of hUC-MSCs in vivo, a cyclophosphamide-induced rat model of primary ovarian insufficiency (POI) was established as described in Figure 3A. Following cyclophosphamide treatment, vaginal cytology examination revealed disruption of normal estrous cyclicity. Compared with control animals, POI rats displayed prolonged diestrus phases and less distinct estrous phases, indicating impaired ovarian function (data not shown). Gross weight examination demonstrated that ovaries from POI rats were noticeably smaller than those from control animals (Figure 3B, POI *vs* CON). Histological analysis further revealed a significant reduction in the number of developing follicles in the POI group (Figure 4A**,** POI *vs* CON). Consistent with these pathological changes, serum FSH concentrations were significantly increased, whereas AMH and P4 levels were markedly reduced (Figure 4B**,** POI *vs* CON), confirming successful establishment of the POI model.

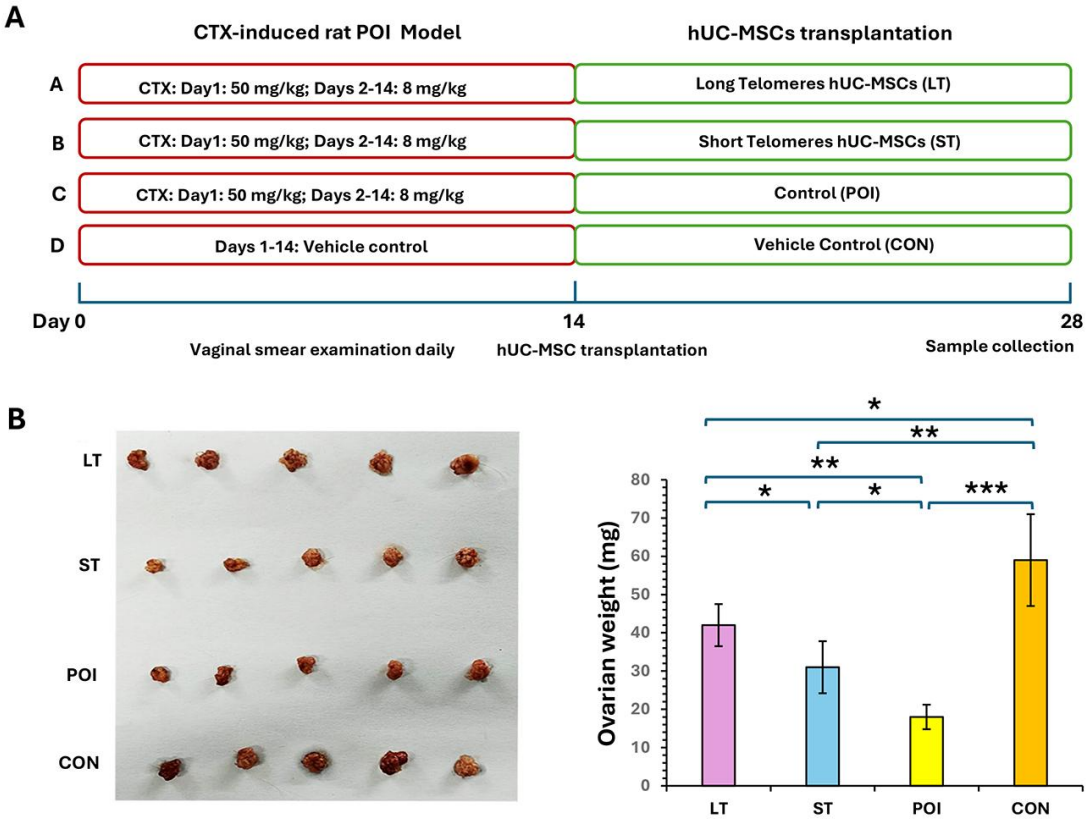
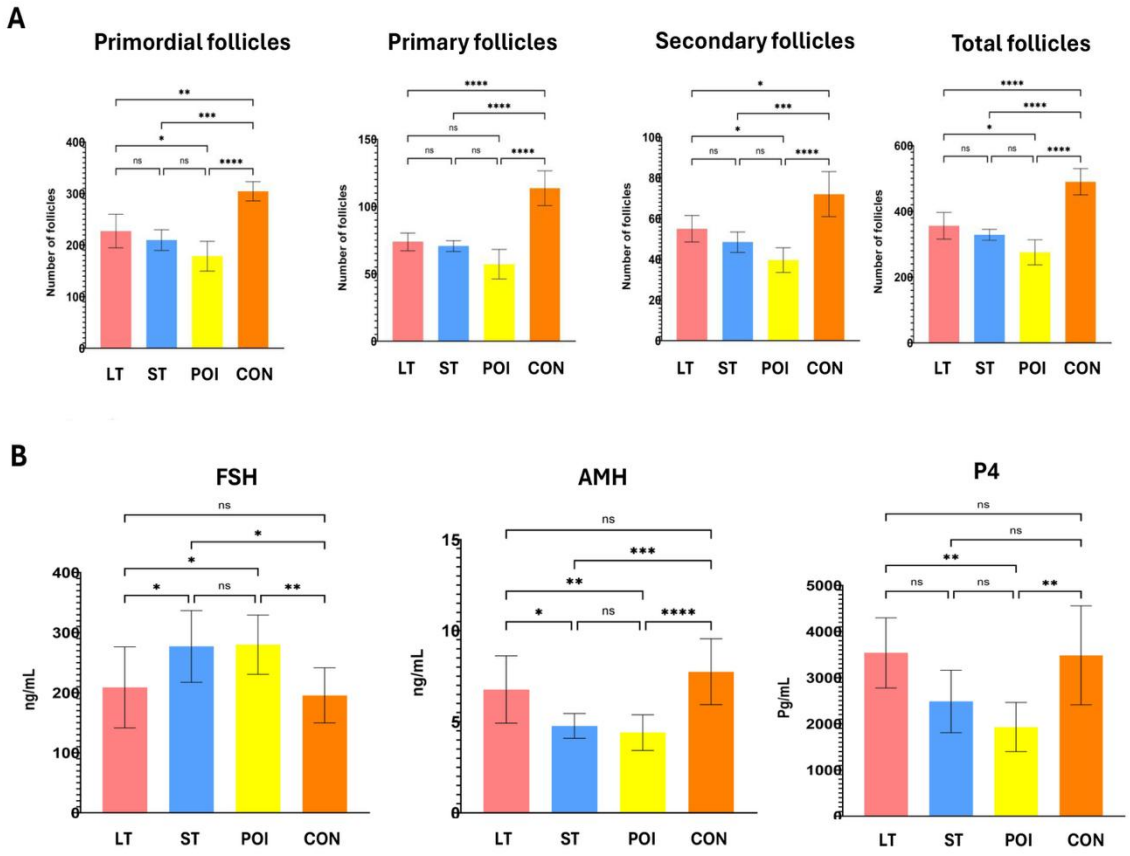


Figure 3. Effects of telomere length in hUC-MSCs on ovarian weight in a rat model of primary ovarian insufficiency. **A**. Schematic illustration of the establishment of the POI model and the transplantation of human umbilical cord mesenchymal stem cells (hUC-MSCs). **B.** Representative photographs of ovaries from POI rats transplanted with Long Telomere hUC-MSCs (LT), Short Telomere hUC-MSC (ST), and vehicle (POI), and age-matched untreated control (CON) are shown (left panel). Quantitative analysis of ovarian weight is presented as mean ± SD **(**right panel, n=5). Statistical significance is indicated as follows: $P < 0.05$ (*), $P < 0.01$ (**), and $P < 0.001$(***).

403 The therapeutic effects of hUC-MSCs possessing different telomere lengths were subsequently
404 evaluated by ovarian transplantation. As shown in Figure 3B, a significant increase in the
405 ovarian weights was observed in both hUC-MSC-treated groups when compared with
406 untreated POI animals (LT *vs* POI, ST *vs* POI), and the increase was greater in the long-
407 telomere group than that in the short-telomere group (LT *vs* ST). Histological analysis
408 demonstrated that transplantation of short telomere hUC-MSCs did not affect the total numbers
409 of follicles at any developing stages compared with untreated POI rats (Figure 4A**,** ST *vs* POI).
410 No significant difference in the number of primordial and primary follicles was observed in the
411 ovaries transplanted with long telomere hUC-MSCs. Interestingly, the number of the secondary
412 follicles and the total number of follicles were significantly increased in response to long
413 telomere cells (Figure 4A). In addition, animals receiving long-telomere hUC-MSCs exhibited
414 lower serum FSH levels and higher AMH and progesterone levels compared to POI animals,
415 as well as animals received short-telomere hUC-MSCs (Figure 4B**,** LT *vs* POI; LT *vs* ST).

416 The ovulation potential in these females was also evaluated in a subset of animals following
417 ovarian transplantation of hUC-MSCs (n=5 per group). Female rats were primed with PMSG
418 administration, ovulation was induced by hCG. As shown in Figure 5, compared to the normal
419 number of the ovulated eggs in the control animals (34 in average), only 2 eggs were observed
420 in POI rat group. Interestingly, compared to POI animals the numbers of the ovulated eggs
421 were increased in short-telomere group (15 *vs* 2), and increased even more in the long-telomere
422 group (22 in average). Collectively, these findings demonstrate that hUC-MSC transplantation
423 effectively ameliorates ovarian dysfunction in cyclophosphamide-induced POI rats, hUC-
424 MSCs with longer telomeres possess even higher therapeutic efficacy.

425



426 **Figure 4.** Effects of telomere length in hUC-MSCs on ovarian morphology and hormone levels
427 in a rat model of primary ovarian insufficiency.

428 Ovarian sections and blood samples obtained from POI rats transplanted with long-telomere
429 human umbilical cord mesenchymal stem cells (LT), short-telomere hUC-MSCs (ST), or
430 vehicle (POI) were subjected to histological evaluation (**A**) and hormone measurements (**B**).
431 Age-matched healthy rats served as the untreated control group (CON). (**A).** Ovarian follicle
432 numbers at the primordial, primary, and secondary stages were quantified. **(B)** Serum levels of
433 follicle-stimulating hormone (FSH), anti-Müllerian hormone (AMH), and progesterone (P4)
434 were measured, Data are presented as mean ± SD (n=5). Statistical significance is indicated as
435 follows: $P < 0.05$ (*), $P < 0.01$ (**), $P < 0.001$ (***), and $P < 0.0001$ (****).

436

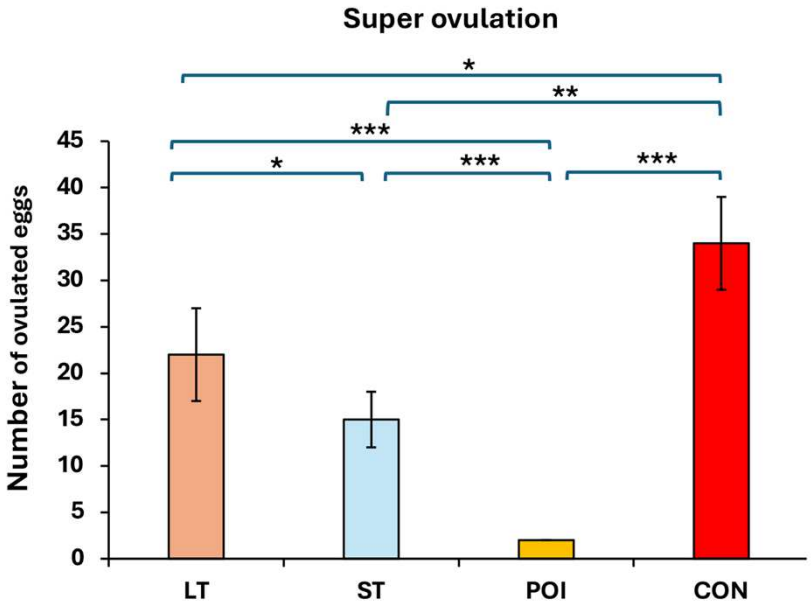


Figure 5. Effects of telomere length in hUC-MSCs on ovulation potential in a rat model of primary ovarian insufficiency.

POI rats transplanted with long-telomere human umbilical cord mesenchymal stem cells (LT), short-telomere hUC-MSCs (ST), or vehicle (POI) were primed with PMSG for 48 hours, ovulation was induced by hCG administration. 13-15 hours later the ovulated eggs were examined in ampulla microscopically and quantified. Age-matched healthy rats served as the untreated control group (CON). Data are presented as mean ± SD (n=5 per group). Statistical significance is indicated as follows: $P < 0.05$ (*), $P < 0.01$ (**), and $P < 0.001$ (***).

Expression of CXCL6 and INHBA in the ovaries transplanted with hUC-MSCs

Proteomic analyses demonstrated significantly higher levels of CXCL6 and INHBA in the conditioned media collected from long-telomere hUC-MSCs compared with that from short-telomere cells. To investigate their expression in vivo, immunofluorescence staining was performed on ovarian sections collected from POI rats transplanted with hUC-MSCs with different lengths of telomeres. As shown in Figure 6, Positive staining of CXCL6 was primarily localized to the developing follicles and the newly formed corpus luteum structures in the ovaries of untreated rats (Figure 6, Panel D). The immunoreactivity was marked diminished in ovarian tissues obtained from POI animals (Figure 6, panel C). In contrast, CXCL6 expression increased following hUC-MSC transplantation (Figure 6, panel A and B) and was more prominent in animals receiving long-telomere hUC-MSCs (Figure 6, panel A). Similarly, the overall INHBA expression was markedly reduced in POI ovaries **(**Figure 7**,** panel C**)**. Transplantation of hUC-MSCs significantly restored ovarian INHBA expression (Figure 7, panels A and B), with the highest staining intensity was observed in the long-telomere group (Figure 7, panel A).

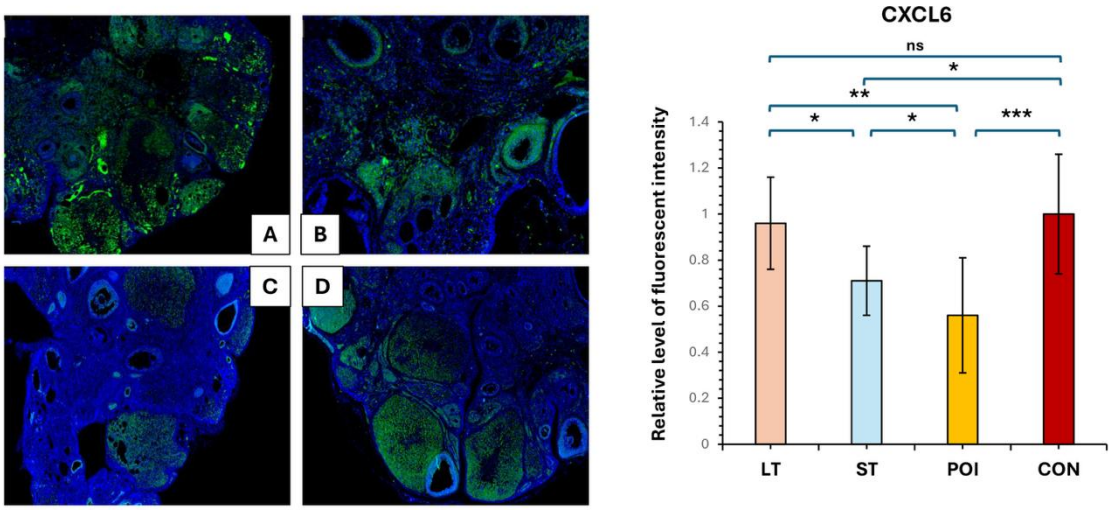


Figure 6. Effects of telomere length in hUC-MSCs on ovarian CXCL6 expression in a rat model of primary ovarian insufficiency. Ovarian sections obtained from POI rats transplanted with long-telomere hUC-MSCs (LT, Panel A), short-telomere hUC-MSCs (ST, Panel B), or vehicle (POI, Panel C) were subjected to immunofluorescence analysis using specific antibodies against CXCL6. Age-matched healthy rats served as the untreated control group (CON, Panel D). The fluorescent intensity was analysed by Image J software, Data are presented as mean ± SD (N=5 for each group). Statistical significance is indicated as follows: $P < 0.05$ (*), $P < 0.01$ (**), and $P < 0.001$ (***). *NS*, no significant difference. Scale bar =100 μm.

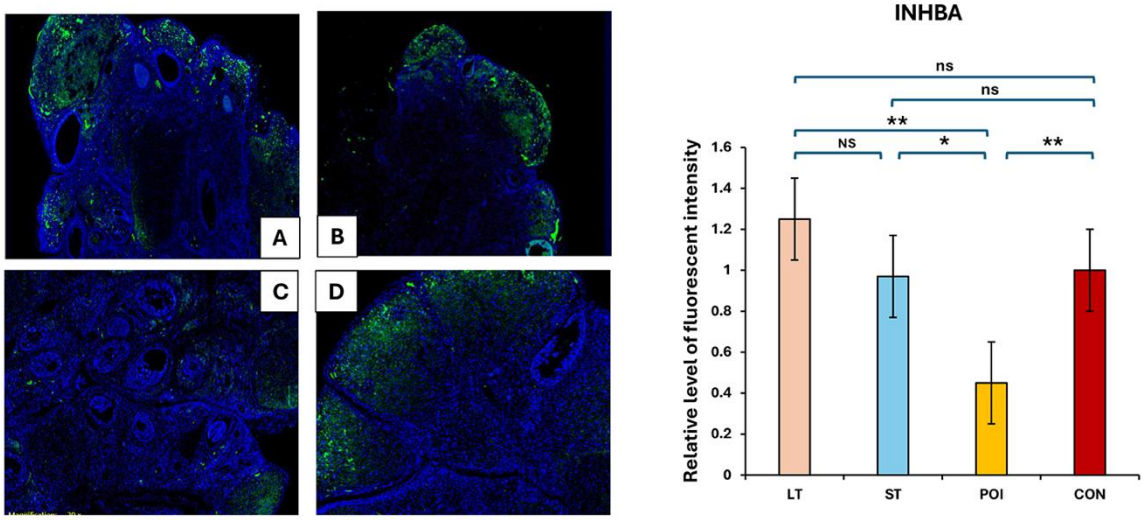


Figure 7. Effects of telomere length in hUC-MSCs on ovarian INHBA expression in a rat model of primary ovarian insufficiency.

Ovarian sections obtained from POI rats transplanted with long-telomere hUC-MSCs (LT, Panel A), short-telomere hUC-MSCs (ST, Panel B), or vehicle (POI, Panel C) were subjected to immunofluorescence analysis using specific antibody against INHBA. Age-matched healthy rats served as the untreated control group (CON, Panel D). The fluorescent intensity was analysed by Image J software, Data are presented as mean ± SD (N=5 for each group). Statistical significance is indicated as follows: $P < 0.05$ (*), $P < 0.01$ (**), and $P < 0.001$ (***). *NS*, no significant difference. Scale bar =100 μm.

Discussion

Telomere length is closely linked to the biological properties of mesenchymal stem cells. Cells with longer telomeres generally exhibit greater proliferative capacity, enhanced self-renewal potential, and prolonged replicative lifespan, whereas telomere shortening is associated with cellular senescence, reduced regenerative capacity, and functional decline [24][25]). In the present study, we explored the association of the proliferative, migratory, differentiation, and secretory properties of hUC-MSCs with lengths of telomeres. Their therapeutic efficacy was assessed in a cyclophosphamide-induced rat model of POI. Our findings demonstrated that hUC-MSCs with longer telomeres exhibit a distinct secretory profile and superior therapeutic efficacy in restoring ovarian function, as evidenced by improved endocrine function, enhanced follicular survival, and better preservation of ovarian reserve. These results indicate that telomere length is a critical determinant of biological function and therapeutic potential in hUC-MSC.

Interestingly, DIA-based proteomic analysis revealed that the overall secretome composition was highly conserved between hUC-MSC populations regardless the telomere length. More than 99% of the identified proteins were shared between the two groups, reflecting the consistency and reliability of hUC-MSC preparations derived from Wharton's jelly. Pearson correlation analysis and principal component analysis further demonstrated strong intra-group correlation but clearly distinguished between the long- and short-telomere groups. These findings suggest that although the core secretory characteristics of hUC-MSCs remain relatively stable, telomere length is associated with quantitative alterations in specific functional proteins.

Among 204 differentially expressed proteins were identified, 66 proteins were upregulated and 138 proteins were downregulated in long-telomere hUC-MSCs. Functional enrichment

517 analyses indicated that these upregulated proteins were primarily involved in immune and
518 inflammatory responses, extracellular matrix remodelling, cell adhesion, signal transduction,
519 apoptosis, and cellular communication. Notably, proteins enriched in the secretome of longer
520 telomere hUC-MSCs include CXCL6, PTX3, FCGR2A, and IFITM1, which are implicated in
521 immune regulation and inflammatory signalling; LOXL1, BMP1, and Decorin, which play
522 critical roles in extracellular matrix organization and tissue remodelling. These observations
523 suggest that telomere length influences a broad range of biological pathways that shape the
524 paracrine functions of hUC-MSCs. Through modulation of immune responses, inflammatory
525 processes, and tissue repair mechanisms, longer telomeres may preserve a more regenerative
526 secretory phenotype, thereby enhancing the therapeutic effects of hUC-MSCs [26].

527 Our proteomic data identified increased expression of INHBA in long-telomere hUC-MSCs,
528 suggesting a potential role for activin/inhibin signalling in ovarian repair. INHBA encodes the
529 inhibin βA subunit, a member of the transforming growth factor-β (TGF-β) superfamily[27].
530 In the ovary, INHBA is predominantly expressed in granulosa cells of developing follicles and
531 plays essential roles in folliculogenesis, granulosa cell proliferation, steroidogenesis, and
532 regulation of follicle-stimulating hormone (FSH) activity through activin signalling. Granulosa
533 cell dysfunction and follicular depletion are frequently associated with reduced INHBA
534 expression and impaired activin signalling[28]. In women with POI, the loss of functional
535 follicles and granulosa cell injury are accompanied by diminished inhibin/activin signalling
536 and elevated circulating FSH concentrations [29]. Disruption of this feedback mechanism
537 contributes directly to the characteristic of POI [30,31]. In the present study,
538 immunofluorescence analysis demonstrated restoration of ovarian INHBA expression
539 following hUC-MSC transplantation, particularly in animals receiving long-telomere hUC-
540 MSCs. These findings suggest that long-telomere hUC-MSCs may facilitate follicular recovery,
541 at least in part, through modulation of INHBA-related signalling pathways. Consequently,

enhanced INHBA secretion may contribute to the observed reduction in serum FSH levels and improvement in ovarian endocrine function.

Another intriguing finding was the increased expression of CXCL6 in long-telomere hUC-MSCs. CXCL6 is a CXC chemokine primarily recognized for its role in neutrophil recruitment. Although CXCL6 is expressed at relatively low levels in normal ovarian tissue, growing evidence indicates that chemokine-mediated immune signalling is essential for ovarian homeostasis, contributing to folliculogenesis, ovulation-associated inflammation, and immune cell recruitment within the ovary[32]. Therefore, increased CXCL6 secretion by long-telomere hUC-MSCs may contribute to tissue remodelling, follicular development, and luteal formation through modulation of local inflammatory environment.

Emerging transcriptomic studies revealed altered CXCL6 expression in several ovarian disorders, including polycystic ovary syndrome, ovarian aging, and ovarian cancer. However, the functional significance of CXCL6 in ovarian regeneration remains poorly understood. In the present study, enhanced level of CXCL6 protein was observed both in the conditioned medium of long-telomere hUC-MSCs and in ovarian tissues following transplantation. Although these findings suggest a potential role for CXCL6 in ovarian repair, further mechanistic studies will be required to clarify its contribution to follicular recovery and restoration of ovarian function.

Taken together, our results demonstrate that hUC-MSCs with longer telomeres exhibit superior therapeutic efficacy in a rat model of POI. The enhanced regenerative capacity of these cells appears to be associated with the altered secretory protein profile, including those that are involved in tissue remodelling, immune regulation, and ovarian function. These findings suggest that telomere length may serve as a valuable biomarker for assessing the quality and therapeutic potency of MSC products in regenerative medicine.

Nevertheless, several limitations of this study should be acknowledged. The interactions among transplanted hUC-MSCs, ovarian cells, and the local tissue microenvironment are highly complex, and the precise molecular mechanisms underlying the therapeutic effects of long-telomere hUC-MSCs remain incompletely understood. In addition, long-term safety, cell fate determination, reproductive outcomes, and the potential off-target effects were not assessed in the present study. Future investigations incorporating mechanistic analyses, lineage-tracing approaches, and long-term efficacy and safety evaluations will be essential to elucidate the mechanisms of action of hUC-MSCs in restoration of the ovarian functions and to facilitate the clinical translation of hUC-MSC-based therapy for patients with POI.

Declarations

Abbreviations

AMH, Anti-Müllerian hormone; CTX, cyclophosphamide; CXCL6, C-X-C motif chemokine ligand 6; DEPs, Differentially expressed proteins; DIA, data -independent acquisition; E2, 17β-estradiol; FDR, false discovery rate; FSH, Follicle-stimulating hormone; hUC-MSCs, Human umbilical cord-derived mesenchymal stem cells; INHBA, Inhibin beta A; KEGG, Kyoto Encyclopedia of Genes and Genomes pathway analysis; MHC-II/HLA class II, major histocompatibility complex; class II; P4, Progesterone; POI, primary ovarian insufficiency.

Ethics approval and consent to participate

The human umbilical cord tissue used for isolation of hUC-MSCs was obtained from healthy full-term deliveries after written informed consent mothers, and the study was conducted in accordance with the principles of the Declaration of Helsinki and was approved by the Ethics Committee of Changzhi Medical College (Approval No. 2021-043).

Animals were housed under standard laboratory conditions with free access to food and water. All procedures were approved by the Institutional Animal Care and Use Committee of Changzhi Medical College (Approval No. DW2021098).

Consent for publication

All authors read and approved the manuscript prior to submission.

Availability of data and materials

Original data generated and analysed during this study are included in this published article. The mass spectrometry proteomics data have been deposited to the ProteomeXchange Consortium via the PRIDE partner repository, and the dataset is publicly available with identifier PXD082583.

Competing Interests

The authors declare no conflict of interest exists.

Funding

This research was funded by National Natural Science Foundation of China, 31971073 to Dr. Li, and Natural Science Foundation of Shanxi Province NSF201901D111 328 to Dr. Miao.

Authors' contributions

HB and WH share equal contribution to this study. The manuscript was written by WH and QL. Experiments were designed by HB, WH, CM and QL, and performed by WH and ZW. Data analysis was performed by WH and QL.

Acknowledgements

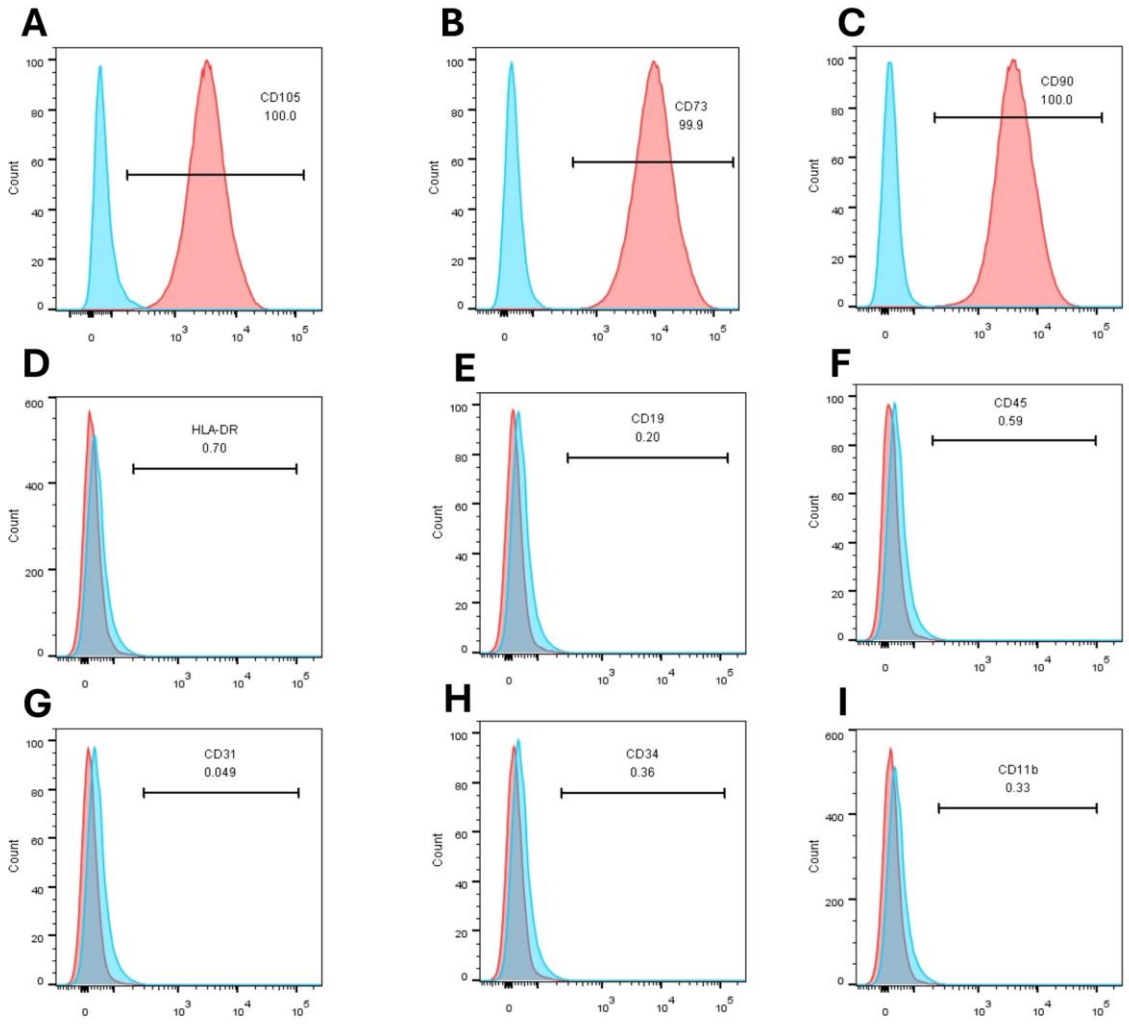
The authors would like to thank Rensheng Yang, Haorui Wang and Zixuan Jia for their assistance in this study.

Figures and Tables:

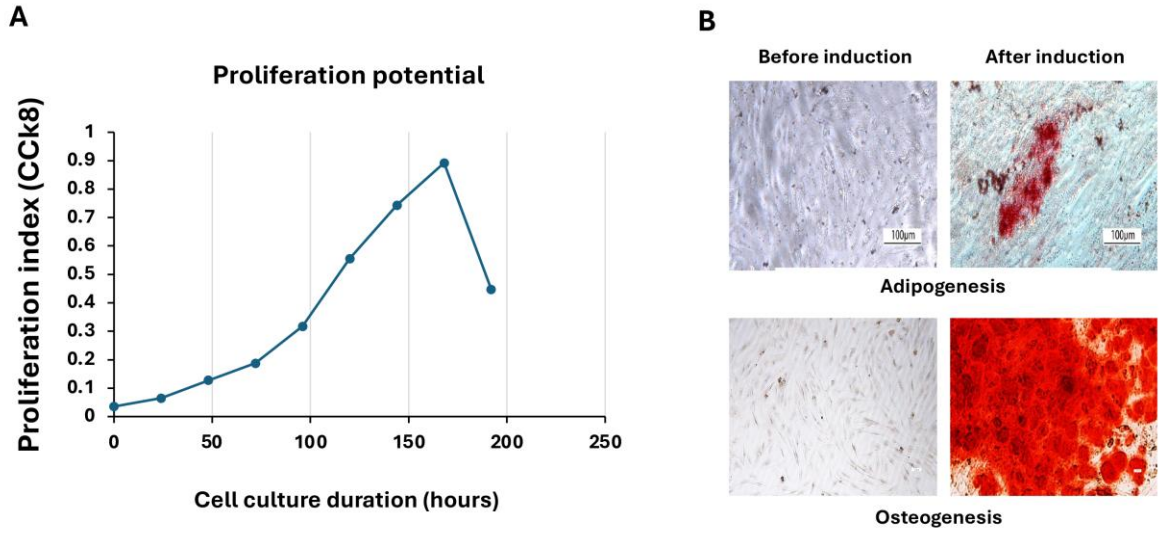
Supplementary Table S1. Antibodies used in this study

Marker	Catalog No.	RRID	Supplier
CD73	E-AB-F1242E-20T	AB_3753365	Elabscience Biotechnology Co., Ltd., Wuhan, China
CD90	E-AB-F1167J-20T	AB_3753364	Elabscience Biotechnology Co., Ltd., Wuhan, China
CD105	E-AB-F1310D-20T	AB_3753366	Elabscience Biotechnology Co., Ltd., Wuhan, China
CD34	E-AB-F1143C	AB_3753370	Elabscience Biotechnology Co., Ltd., Wuhan, China
CD45	E-AB-F1137C	AB_3753369	Elabscience Biotechnology Co., Ltd., Wuhan, China
CD19	E-AB-F1004C	AB_3753367	Elabscience Biotechnology Co., Ltd., Wuhan, China
CD11b	E-AB-F1146C	AB_3753371	Elabscience Biotechnology Co., Ltd., Wuhan, China
HLA-DR	E-AB-F111C-20T	AB_3753363	Elabscience Biotechnology Co., Ltd., Wuhan, China
CD31	E-AB-F1050C	AB_3753368	Elabscience Biotechnology Co., Ltd., Wuhan, China
INHBA	PA5-95909	AB_2807711	Thermo Fisher Scientific,USA
CXCL6	PA5-115276	AB_2899912	Thermo Fisher Scientific,USA

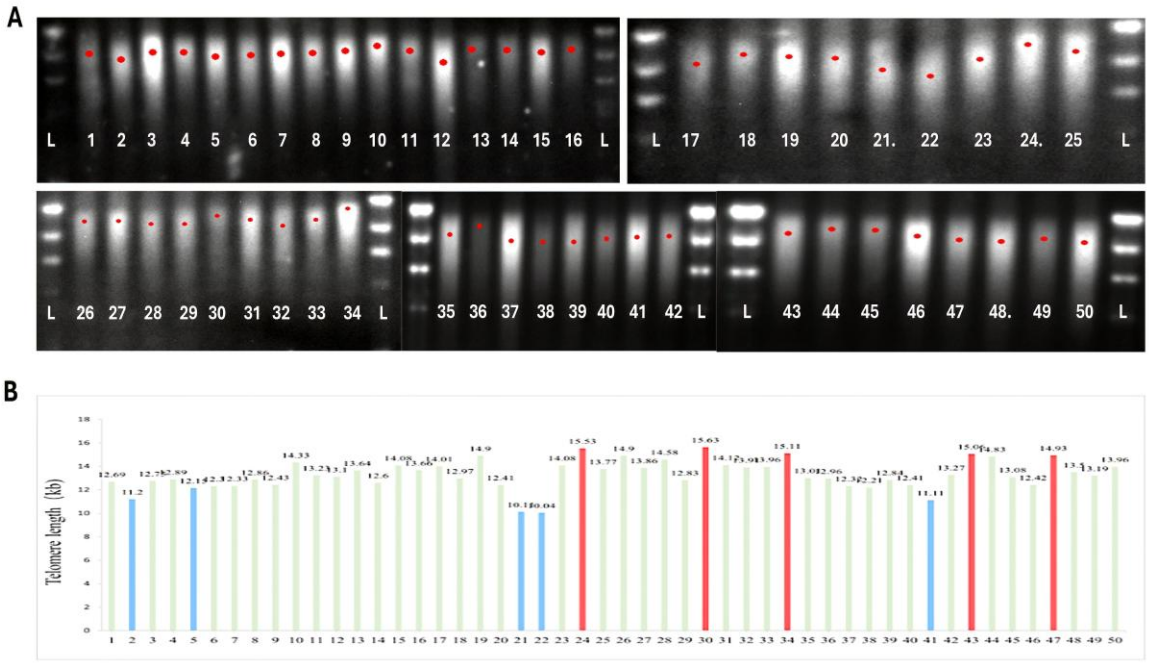
Supplementary Figure S1. Immunophenotypic characterization of hUC-MSCs by flow cytometry showing positive expression of CD105 (A), CD 73 (B), and CD90 (C) and negative expression of HLA-DR (D), CD10 (E), CD45 (F), CD31 (G), CD 34 (H), and CD11b (I).



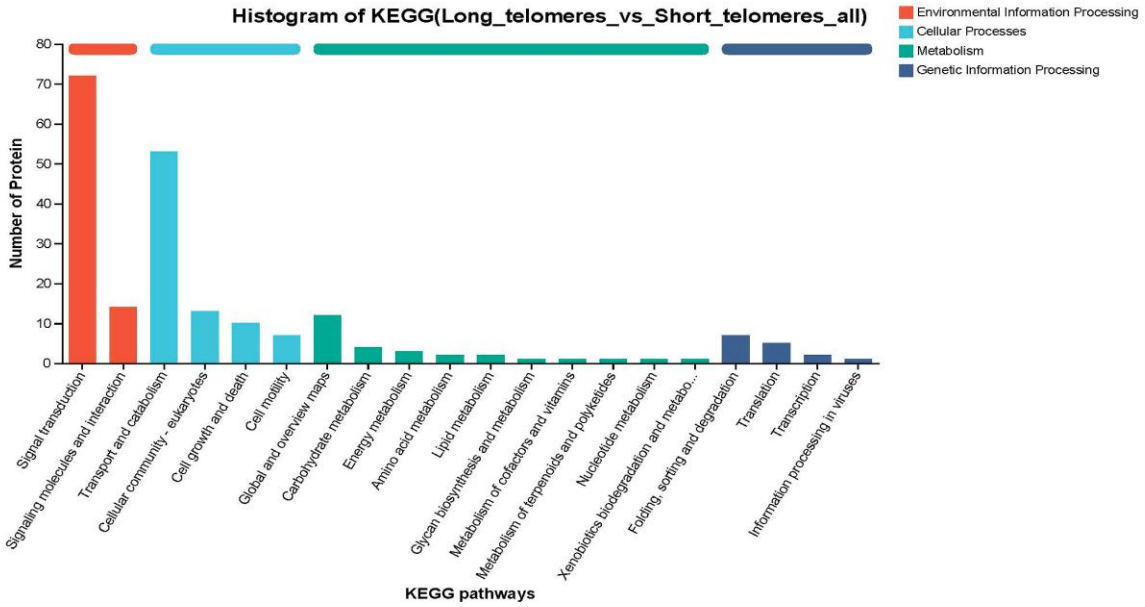
Supplementary Figure S2. Proliferation and differentiation potentials of hUC-MSCs. **(A).** Growth curve of cultured MSCs showing progressive cell proliferation during culture. **(B)** Adipogenic differentiation assessed by Oil Red O staining and osteogenic differentiation assessed by Alizarin Red S staining. Representative micrographs show abundant accumulation of intracellular lipid droplets following adipogenic induction (upper panel, red stain), or calcium-rich mineralized nodules after osteogenic induction (lower, panel, red stain). Scale bars = 100 μm.



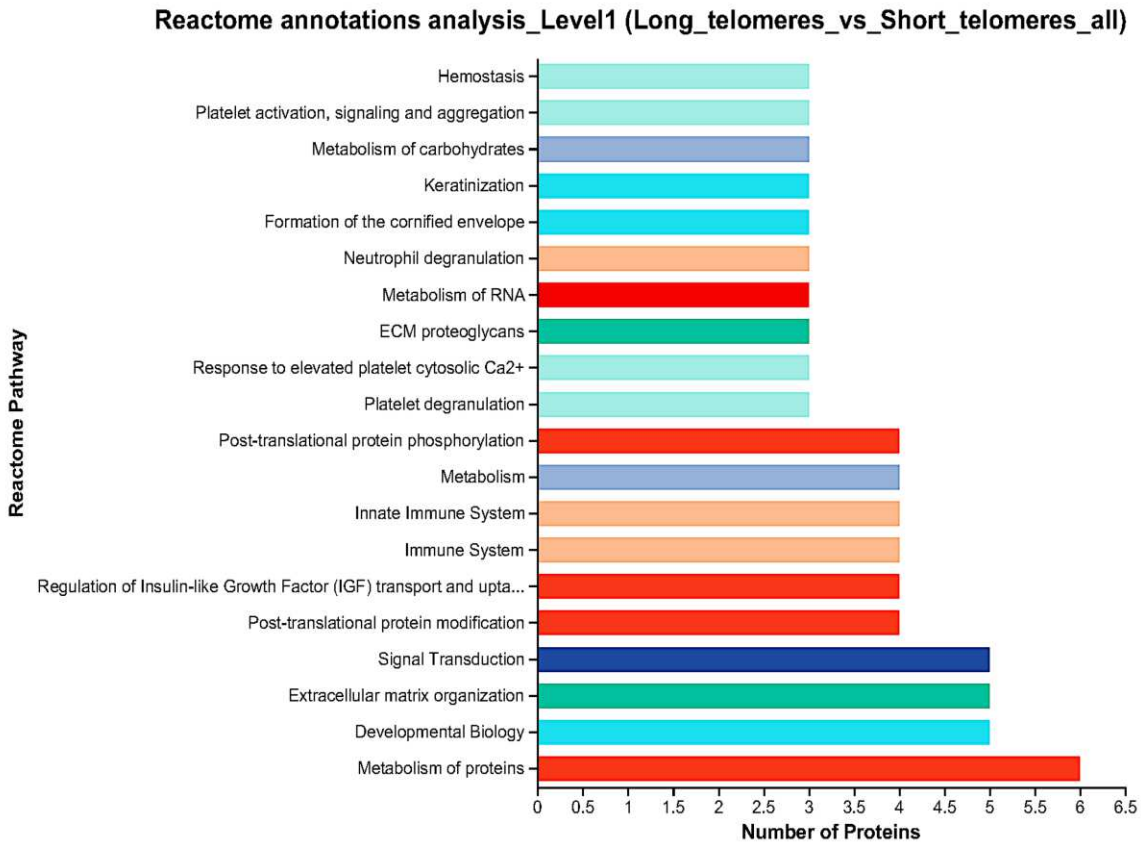
Supplementary Figure S3. Telomere length measurement in 50 hUC-MSCs samples. **(A).** Terminal restriction fragment assay. Genomic DNA was subjected to enzymatic digestion and analysed by Southern blot hybridization. **(B)**. Telomere lengths are measured by TeloTool software and presented as kilobase pairs. 5 samples with the longest telomere lengths are highlighted in red. 5 samples with the shortest telomere lengths are highlighted in blue.



Supplementary Figure S4. KEGG pathway enrichment analysis of differentially expressed proteins in the secretome of hUC-MSCs with the longest and shortest telomeres. Differentially expressed proteins identified in the conditioned media of hUC-MSCs with the longest versus shortest telomeres were subjected to Kyoto Encyclopedia of Genes and Genomes (KEGG) pathway enrichment analysis. The significantly enriched pathways are presented according to enrichment score and significance level.



Supplementary Figure S5. Reactome pathway enrichment analysis of differentially secreted proteins in hUC-MSCs with the longest and shortest telomeres. Differentially expressed proteins identified in the conditioned media of hUC-MSCs with the longest versus shortest telomeres were subjected to Reactome pathway enrichment analysis.



694 **Reference**

695

696 [1] Ding DC, Chang YH, Shyu WC, Lin SZ. Human umbilical cord mesenchymal stem cells:
697 a new era for stem cell therapy. Cell Transplant 2015; 24:339–347.

698 [2] Arutyunyan I, Elchaninov A, Makarov A, Fatkhudinov T. Umbilical Cord as
699 Prospective Source for Mesenchymal Stem Cell-Based Therapy. Stem Cells Int 2016;
700 2016.

701 [3] Stefańska K, Ożegowska K, Hutchings G, Popis M, Moncrieff L, Dompe C, Janowicz
702 K, Pieńkowski W, Gutaj P, Shibli JA, Prado WM, Piotrowska-Kempisty H, et al. Human
703 Wharton's Jelly-Cellular Specificity, Stemness Potency, Animal Models, and Current
704 Application in Human Clinical Trials. J Clin Med 2020; 9.

705 [4] Bharti D, Shivakumar SB, Park JK, Ullah I, Subbarao RB, Park JS, Lee SL, Park BW,
706 Rho GJ. Comparative analysis of human Wharton's jelly mesenchymal stem cells
707 derived from different parts of the same umbilical cord. Cell Tissue Res 2018; 372:51–
708 65.

709 [5] Nagamura-Inoue T, He H. Umbilical cord-derived mesenchymal stem cells: Their
710 advantages and potential clinical utility. World J Stem Cells 2014; 6:195.

711 [6] Wang Y, Wang H, Tan J, Cao Z, Wang Q, Wang H, Yue S, Li W, Wang D. Therapeutic
712 effect of mesenchymal stem cells and their derived exosomes in diseases. Molecular
713 Biomedicine 2025; 6.

714 [7] Trigo CM, Rodrigues JS, Camões SP, Solá S, Miranda JP. Mesenchymal stem cell
715 secretome for regenerative medicine: Where do we stand? J Adv Res 2025; 70:103–124.

[8] Nethaji K, Ashiq Shibili P, Dey A, Nambidi S, Banerjee A, Barbon S, Pathak S, Duttaroy AK. Therapeutic applications of human umbilical cord-derived mesenchymal stem cell secretome in chronic inflammatory diseases and cancer: A recent update. Mol Immunol 2026; 190:140–151.

[9] Li X, Zhang D, Yu Y, Wang L, Zhao M. Umbilical cord-derived mesenchymal stem cell secretome promotes skin regeneration and rejuvenation: From mechanism to therapeutics. Cell Prolif 2024; 57.

[10] Nelson LM. Clinical practice. Primary ovarian insufficiency. N Engl J Med 2009; 360:606–14.

[11] Touraine P, Chabbert-Buffet N, Plu-Bureau G, Duranteau L, Sinclair AH, Tucker EJ. Premature ovarian insufficiency. Nat Rev Dis Primers 2024; 10.

[12] Zhao Y, Ma J, Yi P, Wu J, Zhao F, Tu W, Liu W, Li T, Deng Y, Hao J, Wang H, Yan L. Human umbilical cord mesenchymal stem cells restore the ovarian metabolome and rescue premature ovarian insufficiency in mice. Stem Cell Res Ther 2020; 11.

[13] Li Z, Zhang M, Zheng J, Tian Y, Zhang H, Tan Y, Li Q, Zhang J, Huang X. Human Umbilical Cord Mesenchymal Stem Cell-Derived Exosomes Improve Ovarian Function and Proliferation of Premature Ovarian Insufficiency by Regulating the Hippo Signaling Pathway. Front Endocrinol (Lausanne) 2021; 12.

[14] Umer A, Khan N, Greene DL, Habiba UE, Shamim S, Khayam AU. The Therapeutic Potential of Human Umbilical Cord Derived Mesenchymal Stem Cells for the Treatment of Premature Ovarian Failure. Stem Cell Rev Rep 2023; 19:651–666.

[15] Lv X, Guan C, Li Y, Su X, Zhang L, Wang X, Xia HF, Ma X. Effects of single and multiple transplantations of human umbilical cord mesenchymal stem cells on the recovery of ovarian function in the treatment of premature ovarian failure in mice. J Ovarian Res 2021; 14.

[16] Guo C, Ma Y, Situ Y, Liu L, Luo G, Li H, Ma W, Sun L, Wang W, Weng Q, Wu L, Fan D. Mesenchymal stem cells therapy improves ovarian function in premature ovarian failure: a systematic review and meta-analysis based on preclinical studies. Front Endocrinol (Lausanne) 2023; 14.

[17] Celtikci B, Erkmen GK, Dikmen ZG. Regulation and Effect of Telomerase and Telomeric Length in Stem Cells. Curr Stem Cell Res Ther 2020; 16:809–823.

[18] Lupatov AY, Yarygin KN. Telomeres and Telomerase in the Control of Stem Cells. Biomedicines 2022; 10.

[19] Zheng Y, Wu S, Liu L, Guan Y, Sun W, Miao C, Li Q. Activation of HAND2-FGFR signaling pathway by lncRNA HAND2-AS1 in adenomyosis . Biol Reprod 2023.

[20] Mender I, Shay J. Telomere Restriction Fragment (TRF) Analysis. Bio Protoc 2015; 5.

[21] Göhring J, Fulcher N, Jacak J, Riha K. TeloTool: a new tool for telomere length measurement from terminal restriction fragment analysis with improved probe intensity correction. Nucleic Acids Res 2014; 42.

[22] Han C, Shi C, Liu L, Han J, Yang Q, Wang Y, Li X, Fu W, Gao H, Huang H, Zhang X, Yu K. Majorbio Cloud 2024: Update single-cell and multiomics workflows. IMeta 2024; 3.

[23] Li H, Song D, Zhong Y, Qian C, Zou Q, Ou J, Shi Y, Gao L, Wang G, Liu Z, Li H, Ding H, et al. Human Umbilical Cord Mesenchymal Stem Cells Therapy in Cyclophosphamide-Induced Premature Ovarian Failure Rat Model. Biomed Res Int 2016; 2016.

[24] Hannon PR, Peretz J, Flaws JA. Daily exposure to Di(2-ethylhexyl) phthalate alters estrous cyclicity and accelerates primordial follicle recruitment potentially via dysregulation of the phosphatidylinositol 3-kinase signaling pathway in adult mice. Biol Reprod 2014; 90.

[25] Trivanović D, Jauković A, Popović B, Krstić J, Mojsilović S, Okić-Djordjević I, Kukolj T, Obradović H, Santibanez JF, Bugarski D. Mesenchymal stem cells of different origin: Comparative evaluation of proliferative capacity, telomere length and pluripotency marker expression. Life Sci 2015; 141:61–73.

[26] Lupatov AY, Yarygin KN. Telomeres and Telomerase in the Control of Stem Cells. Biomedicines 2022; 10.

[27] Siraj Y, Galderisi U, Alessio N. Senescence induces fundamental changes in the secretome of mesenchymal stromal cells (MSCs): implications for the therapeutic use of MSCs and their derivates. Front Bioeng Biotechnol 2023; 11:1148761.

[28] de Kretser DM, O'Hehir RE, Hardy CL, Hedger MP. The roles of activin A and its binding protein, follistatin, in inflammation and tissue repair. Mol Cell Endocrinol 2012; 359:101–106.

[29] Jiao X, Meng T, Zhai Y, Zhao L, Luo W, Liu P, Qin Y. Ovarian Reserve Markers in Premature Ovarian Insufficiency: Within Different Clinical Stages and Different Etiologies. Front Endocrinol (Lausanne) 2021; 12.

[30] Chon SJ, Umair Z, Yoon MS. Premature Ovarian Insufficiency: Past, Present, and Future. Front Cell Dev Biol 2021; 9.

[31] Cacciottola L, Camboni A, Dolmans MM. Immune system regulation of physiological and pathological aspects of the ovarian follicle pool throughout the female reproductive lifespan. Hum Reprod 2025; 40:12–22.

Supplementary Files

This is a list of supplementary files associated with this preprint. Click to download.

- SupplementaryFigureS1.tif
- SupplementaryFigureS2.tif
- SupplementaryFigureS3.tif
- SupplementaryFigureS4.tif
- SupplementaryFigureS5.tif
- SupplementaryFigureS6.pdf
- SupplmentarytableS1.docx